


Research

Whale Optimization Algorithm for structural damage detection, localization, and quantification

Daniele Kautz Monteiro¹  · Letícia Fleck Fadel Miguel²  · Gustavo Zeni³ · Tiago Becker⁴ · Giovanni Souza de Andrade⁵ · Rodrigo Rodrigues de Barros⁵

Received: 27 May 2024 / Accepted: 18 September 2024

Published online: 10 October 2024

© The Author(s) 2024 

Abstract

This paper introduces an approach for vibration-based damage detection based on matrix updating aided by the Whale Optimization Algorithm (WOA). The methodology uses the Data-driven Stochastic Subspace Identification (SSI-DATA) technique to determine the modal parameters, which are compared with those obtained from both healthy and damaged conditions of the structure. The methodology's efficacy is assessed through three distinct steps: numerical simulations, experimental data, and real-world data from a bridge. Initially, numerical analyses are conducted on a cantilever beam, a 10-bar truss, and a Warren truss subjected to environmental vibrations with varying damage cases and noise levels. Subsequently, experimental validations are performed on a test system and in the Z24 Bridge. Results from the computational simulations demonstrate the method's promise to identify, locate, and quantify single and multiple damage cases, even amidst signal noise, variations in the first vibration mode as minimal as 0.015%, and complex structures with 54 elements. Moreover, the matrix updating method utilizing WOA showcased superior accuracy compared to existing techniques in the literature. In addition, the Z24 Bridge example validated the capability of the presented damage detection method to localize structural damage solely based on natural frequencies.

Keywords Structural Health Monitoring (SHM) · Damage detection · Damage localization · Damage quantification · Whale Optimization Algorithm (WOA)

1 Introduction

The integrity of civil structures is crucial, as damage resulting from natural degradation or unforeseen events can cause catastrophic accidents. Hence, Structural Health Monitoring (SHM) is a critical subject that offers continuous monitoring to ensure user safety. SHM primarily relies on vibration-based methods, which involve monitoring

✉ Daniele Kautz Monteiro, daniele.kautz@ufrgs.br; danielekautz@hotmail.com; ✉ Letícia Fleck Fadel Miguel, letffm@ufrgs.br; Gustavo Zeni, gustavo.zeni@ufrgs.br; Tiago Becker, tiago.becker@ufrgs.br; Giovanni Souza de Andrade, giovanni.andrade@ufrgs.br; Rodrigo Rodrigues de Barros, rodrigo.barros@ufrgs.br | ¹Graduate Program in Civil Engineering (PPGEC), Federal University of Rio Grande Do Sul (UFRGS), Avenida Osvaldo Aranha, 99, Porto Alegre, Rio Grande do Sul 90035-190, Brazil. ²Department of Mechanical Engineering (DEMEC), Graduate Program in Mechanical Engineering (PROMEC), Graduate Program in Civil Engineering (PPGEC), Federal University of Rio Grande Do Sul (UFRGS), Avenida Sarmiento Leite 425, 2º Andar, Porto Alegre, Rio Grande do Sul 90050-170, Brazil. ³Graduate Program in Mining, Metallurgy and Materials Engineering (PPGEM), Federal University of Rio Grande Do Sul (UFRGS), Porto Alegre, Brazil. ⁴Department of Mechanical Engineering (DEMEC), Federal University of Rio Grande Do Sul (UFRGS), Porto Alegre, Brazil. ⁵Applied Mechanics Group (GMAp), School of Engineering, Federal University of Rio Grande Do Sul (UFRGS), Porto Alegre, Brazil.



a structure's dynamic responses over time, including displacements, velocities, and accelerations. These methods explore damage-sensitive features to assess structural conditions, e.g., natural frequencies and mode shapes.

Acquiring modal parameters typically involves analyzing experimental data derived from structural responses through system identification processes. Since structures like bridges and buildings are often subject to random excitation sources (such as wind, traffic, and human activities), employing stochastic system identification methods under output-only measurement conditions is imperative. Frequency or time domain techniques are commonly utilized for in situ measurements in SHM applications. These include the Eigensystem Realization Algorithm (ERA) method [1], the Stochastic Subspace Identification (SSI) technique [2], and the poly-reference Least-Squares Complex Frequency domain (p-LSCF) method [3].

Damage detection methods should be applied over the structure's lifespan, considering the construction layout and its intended purpose. These methods leverage damage-sensitive features to assess structural health. Examples include techniques based on alterations in modal parameters [4–6], derivatives of modal parameters [7–9], modal flexibility [10, 11], Bayesian probabilistic inference [12, 13], wavelet transform [14, 15], matrix updating [16–18], and Machine Learning [19–23].

Comprehensive reviews of state-of-the-art structural damage detection methods are provided by [24–26]. Rytter [27] categorizes these approaches into four levels: (i) damage detection, (ii) damage localization, (iii) damage quantification, and (iv) estimation of the remaining service life. While literature primarily focuses on levels (i) to (iii), level (iv) falls under Structural Assessment. Still, no universally accepted method is applicable across all structures or types of damage. Each methodology exhibits its own set of limitations, reinforcing the importance of testing, comparing, and refining damage detection approaches across diverse civil structures to establish effectiveness and efficiency.

In the existing literature, numerous studies often face challenges in achieving all of Rytter's three levels, particularly in complex structures or under varying environmental conditions. For instance, Zheng et al. [13] show that methods with the potential capacity for determining the extent and location of damage may require extensive computational resources. Additionally, methods relying solely on modal parameters can sometimes lead to inaccurate localization due to the limited spatial resolution [4, 6]. These challenges underscore the need for more robust and efficient approaches to address these limitations while ensuring accuracy in real-world applications.

Moreover, damage detection methods rely heavily on comparing information against values obtained under healthy conditions (the reference case). Therefore, methodologies have enhanced predictive capabilities when integrating physical parameters, such as calibrated numerical models ([28, 29]), into the assessment process. Finite Element (FE) models, if effectively representing a structure's modal properties, are a powerful solution alongside other damage detection techniques. One example of a model-based approach involves formulating an optimization problem.

Optimization-based or matrix updating methods modify the system's matrices (stiffness and damping) to reliably reproduce the dynamic or static response from the measured data. In short, the optimization problem is solved using equations of motion and experimental measurements, with the comparison of the original and updated matrices providing a damage identifier. This type of optimization problem is ill-posed, making gradient-based optimization challenging. Therefore, Metaheuristic algorithms have been broadly used in these cases to deal with complex objective functions [30–33].

Within this framework, the present paper proposes an approach to detect, locate, and quantify structural damage utilizing an optimization-based method via the Whale Optimization Algorithm (WOA). The modal parameters (natural frequencies and mode shapes) obtained from ambient vibration are used as damage-sensitive features to achieve all three of Rytter's levels and identify single and multiple damages. In addition, simplified numerical models were used in this work to deal with computational cost problems. Unlike many papers that evaluate damage detection methodologies using numerical examples or basic experiments, this study went further by assessing the presented approach on the Z24 bridge, a benchmark structure. This comprehensive evaluation highlights its potential for practical applications in real-world scenarios.

The methodology was verified across three main groups: (1) simulation of damage cases across three numerical structures subjected to environmental vibrations considering noise levels; (2) experimental testing in a simple system to validate the framework; (3) verification of the method in the Z24 bridge. The paper's structure is as follows. Section 2 describes the damage detection method based on matrix updating via WOA, Sect. 3 exhibits three numerical examples, Sect. 4 presents the analysis of an experiment structure, Sect. 5 shows the bridge's study, and Sect. 6 provides final remarks.

2 Damage detection based on matrix updating

Damage detection methods based on matrix updating solve an optimization problem in which the objective function depends on changes in modal parameters. A FE model compatible with the analyzed structure is required to have a correspondent object with the data obtained experimentally. This comparison seeks to minimize the differences between the parameters identified by the real structure and the model parameters.

To locate and quantify damage cases in this study, the damage was treated as a change in stiffness values. This was accomplished by considering a stiffness reduction factor α_j , which ranges from 0 to 1 – where 1 indicates no damage, and 0 signifies a complete loss of stiffness in element j . Thus, α_j acts on each elemental stiffness matrix \mathbf{k}_j for all N_e elements of the structure:

$$\mathbf{K} = \sum_{j=1}^{N_e} \alpha_j \mathbf{k}_j, \quad (1)$$

in which \mathbf{K} is the global stiffness matrix. The structural damage is estimated by updating the numerical model in which variations are introduced for all α_j factors. This model is continuously modified until the difference with the experimental results is minimized. Therefore, the problem to be solved is a minimization problem defined by:

$$\begin{aligned} &\text{Find } \alpha \\ &\text{Minimize } \Pi(\alpha) = |E - A(\alpha)|^2 \\ &\text{Subject to } 0 \leq \alpha \leq 1, \end{aligned} \quad (2)$$

in which $\Pi(\alpha)$ is the objective function, E is the experimental modal feature extracted from the structure, and $A(\alpha)$ is the analytical modal feature calculated from the numerical model of the structure.

Equation (3) was chosen as the objective function, which was also used by [16, 17, 34]. This equation is based on the natural frequencies and mode shapes obtained analytically and experimentally:

$$\Pi(\alpha) = \sum_{j=1}^{N_m} \left[\left(\frac{\delta\omega_j(\alpha)}{\omega_j} \right)^A - \left(\frac{\delta\omega_j}{\omega_j} \right)^E \right]^2 - \sum_{j=1}^{N_m} \sum_{k=1}^{N_n} \left[(\delta\psi_{kj}(\alpha))^A - (\delta\psi_{kj})^E \right]^2, \quad (3)$$

in which N_m denotes the number of analyzed vibration modes and N_n is the number of nodal displacements. The superscripts A and E refer to analytical and experimental data, respectively. The natural frequencies for the j th mode in both the healthy experimental and analytical conditions are represented by ω_j . The term $\delta\omega_j$ signifies the fractional change in natural frequencies for the j th mode, while $\delta\psi_{kj}$ represents the fractional change in mode shapes for the j th mode of the structure, comparing experimental and analytical data.

The Whale Optimization Algorithm (WOA), summarized in the following section, was used to solve the minimization problem proposed in this work, as this metaheuristic algorithm has proven to be competitive in different types of problems (e.g., [35–39]).

2.1 Whale Optimization Algorithm (WOA)

The WOA is a metaheuristic optimization algorithm developed by Mirjalili and Lewis [40] that mimics the hunting behavior of humpback whales. This behavior is simulated with a random agent or with the best agent in the round chasing the prey. In addition, a spiral is used to simulate whales' bubble-net attack mechanism.

This algorithm assumes that the current best candidate solution is either the target prey or close to the optimal solution. Once the optimal search agent is identified, the positions of the other agents are updated to move toward this optimal agent. This procedure is represented by:

$$\begin{aligned} \bar{D} &= |\bar{C} \cdot \bar{X}^*(t) - \bar{X}(t)| \\ \bar{X}(t+1) &= \bar{X}^*(t) - \bar{A} \cdot \bar{D} \end{aligned} \quad (4)$$

where t is the current iteration, \vec{A} and \vec{C} are coefficient vectors, \vec{X}^* is the position vector of the best solution obtained so far, \vec{X} is the position vector, and \odot represents an element-by-element multiplication. The vectors \vec{A} and \vec{C} are defined as:

$$\begin{aligned}\vec{A} &= 2\vec{a} \cdot \vec{r} - \vec{a} \\ \vec{C} &= 2 \cdot \vec{r},\end{aligned}\quad (5)$$

where \vec{a} is linearly decreased from 2 to 0 over the course of iterations and \vec{r} is a random vector in $[0,1]$.

The whales' bubble-net attack is achieved by the shrinking encircling mechanism and the spiral updating position. The first procedure is generated by decreasing the value of \vec{a} over the iterations. The second occurs by calculating the distance between the whale at (X, Y) and the prey at (X^*, Y^*) , considering a two-dimensional function:

$$\begin{aligned}\vec{X}(t+1) &= \vec{D}' \cdot e^{bl} \cdot \cos(2\pi l) + \vec{X}^*(t) \\ \vec{D}' &= |\vec{X}^*(t) - \vec{X}(t)|,\end{aligned}\quad (6)$$

where b is a constant for defining the shape of the logarithmic spiral and l is a random number in $[-1,1]$.

The whales simultaneously swim around the prey within a shrinking circle and along a spiral path. Mirjalili and Lewis [40] assumed a 50% probability of choosing one of the two paths to update the whales' position in the optimization process in the mathematical model:

$$\vec{X}(t+1) = \begin{cases} \vec{X}^*(t) - \vec{A} \cdot \vec{D} & \text{if } p < 0.5 \\ \vec{D} \cdot e^{bl} \cdot \cos(2\pi l) + \vec{X}^*(t) & \text{if } p \geq 0.5 \end{cases}\quad (7)$$

where p is a random number in $[0,1]$.

Furthermore, the prey's search is also done by the variation of \vec{A} . This vector assumes values over 1 or under -1, making the search agent move far away from a reference whale. In other words, unlike the bubble net attack, the position of the agents in the search for prey is updated randomly instead of using the optimal agent. This step is modeled mathematically using the random position vector \vec{X}_{rand} :

$$\begin{aligned}\vec{D} &= |\vec{C} \cdot \vec{X}_{rand} - \vec{X}| \\ \vec{X}(t+1) &= \vec{X}_{rand} - \vec{A} \cdot \vec{D}\end{aligned}\quad (8)$$

The WOA is summarized by the pseudocode shown in Fig. 1. More details about the WOA can be found in [40].

3 Numerical examples

Numerical simulations of experimental tests on three distinct structures (a cantilever beam, a 10-bar plane truss, and a Warren truss footbridge) were conducted to assess the efficacy of the damage detection approach presented in this study. The first two structures were chosen for comparative analysis with results previously obtained by other researchers, while the inclusion of the third structure allowed for the investigation of multiple damage cases.

Ambient vibration was emulated using white Gaussian noise generated through the Matlab *wgn* function [41]. Subsequently, acceleration responses were computed employing the Newmark Method [42] with an integration $\Delta t = 0.0005$ s. Noise was introduced into the signals using white Gaussian noise via the Matlab *awgn* function [41] to replicate real-world experimental conditions. Finally, the modal parameters necessary for the damage detection methods were obtained using the data-driven Stochastic Subspace Identification (SSI-DATA) method of Peeters [43]. A single signal from each simulated sensor was utilized for the analysis, with one simulated sensor positioned at each degree of freedom in the structural system.

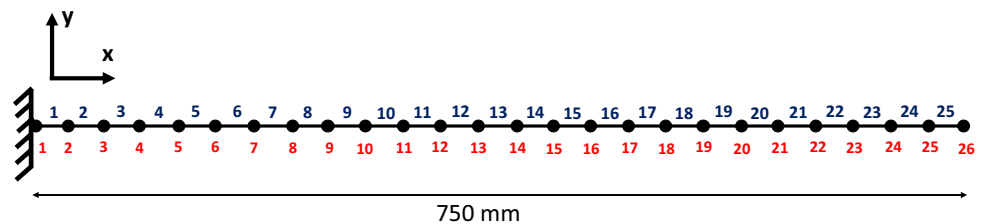
Fig. 1 Pseudo-code of the WOA [40]

```

Initialize the whales population  $X_i$  ( $i = 1, 2, \dots, n$ )
Calculate the fitness of each search agent
 $X^*$  = the best search agent
while ( $j <$  maximum number of iterations)
  for each search agent
    Update  $a$ ,  $A$ ,  $C$ ,  $l$ , and  $p$ 
    if1 ( $p < 0.5$ )
      if2 ( $|A| < 1$ )
        Update the position of the current search agent
      else if2 ( $|A| \geq 1$ )
        Select a random search agent ( $X_{rand}$ )
        Update the position of the current search agent
      end if2
    else if1 ( $p \geq 0.5$ )
      Update the position of the current search agent
    end if1
  end for
  Check if any search agent goes beyond the search space and amend it
  Calculate the fitness of each search agent
  Update  $X^*$  if there is a better solution
   $j = j + 1$ 
end while
return  $X^*$ 

```

Fig. 2 Numerical cantilever beam: 25 finite elements



3.1 Cantilever beam

The initial structure studied was a cantilever beam featuring a square box cross-section with a wall thickness of 1 mm, external dimensions of 25.4 mm, and 750 mm in length. The structure configuration, as analyzed experimentally by Kaminski Jr. and Riera [44], was simulated using 25 Timoshenko beam elements, as illustrated in Fig. 2. The material properties were specified: Poisson's ratio of 0.3, Young's modulus of 68.6 GPa, a Timoshenko shear factor of 0.5, and a specific weight of 28 kN/m³. Additionally, a concentrated mass of 18.2 g was uniformly distributed on each degree of freedom, corresponding to the accelerometers in the experimental setup. Furthermore, a 1% damping ratio was applied in the first and fifth vibration modes to construct the damping matrix.

For the damage cases, it was adopted the three cases studied by Zeni [34]: (1) a 20% stiffness reduction in element 20, (2) a 30% stiffness reduction in element 8, and (3) a 50% stiffness reduction in element 5 and a 30% reduction in element 12. Fadel Miguel et al. [17] and Fadel Miguel et al. [16] analyzed the first two cases. These works employed methodologies based on matrix updating utilizing the optimization algorithms and noise levels.

Tables 1 and 2 present the corresponding natural frequencies derived from the finite element model and stochastic system identification, with noise levels considered in the acceleration responses set at 3% and 5%.

Table 1 Numerical cantilever beam: natural frequencies (Hz)

Mode	FE Model			
	Healthy case	Case 1	Case 2	Case 3
1	26.5600	26.5561	26.2459	25.3154
2	164.3250	163.8733	163.7602	161.3316
3	450.9722	447.0483	445.1953	446.4628

Table 2 Numerical cantilever beam: identified natural frequencies (Hz)

Mode	SSI-DATA (3% noise)				SSI-DATA (5% noise)			
	Healthy case	Case 1	Case 2	Case 3	Healthy case	Case 1	Case 2	Case 3
1	26.5657	26.5622	26.2662	25.3229	26.5657	26.5622	26.2662	25.3229
2	160.8429	160.4204	160.3151	157.9811	160.8425	160.4201	160.3148	157.9808
3	392.3989	389.7449	388.4807	389.3414	392.3984	389.7441	388.4799	389.3406

In both noise scenarios, the initial two frequencies identified by the SSI-DATA technique closely match the FE model's values. However, an error of over 10% was observed from the third frequency, attributed to insufficient participation of the highest frequencies under the influence of the *wgn* function. Consequently, damage detection included only the first three vibration modes.

It was used 100 search agents across 200 iterations for the damage detection method. The outcomes in Figs. 3 and 4 correspond to different noise levels applied to three distinct damage cases. In each case, the damage was accurately located and quantified. The solutions generated by WOA surpassed the results of all mentioned authors [16, 17, 34], reaching more accurate results.

3.2 10-bar plane truss

The following structure studied was a 10-bar plane truss, as depicted in Fig. 5, investigated by Begambre and Laier [45]. Each element within this truss has Young's modulus of 195 GPa, a density of 7700 kg/m³, a cross-section of 4.2 × 10⁻⁴ m², and a moment of inertia of 3 × 10⁻⁸ m⁴. Furthermore, the first and third vibrational modes were subjected to a 1% damping factor.

It examined the scenario involving a 15% stiffness reduction in bars 2 and 8 to compare with the results of [16, 45]. Both studies employed a hybrid optimization approach: [45] combined the PSO and Simplex algorithms, while [16] utilized a hybrid Nelder-Mead algorithm. Consistent with these studies, a 3% noise level was applied to the structural responses for the healthy and damaged cases.

Table 3 presents the natural frequencies derived from the FE model and stochastic system identification. Given the limited truss elements, only the first three modes were utilized for damage detection.

The truss's damage was detected with 50 search agents in 100 iterations. The results of the damage detection methodology are presented in Table 4 alongside the solutions obtained by [16, 45]. The approach utilized in this study effectively identified and quantified the damage case, yielding superior results compared to the solutions provided by the referenced authors.

3.3 Warren truss footbridge

Concluding the numerical analysis, it was analyzed a Warren truss footbridge, obtained from Miguel et al. [46], with a height of 2.23 m and a span of 39 m, as shown in Fig. 6. The material has a specific mass of 7850 kg/m³, Young's modulus of 200 GPa, and a 1% damping ratio in the 1st and 5th vibration modes. The information regarding each bar is given in Table 5.

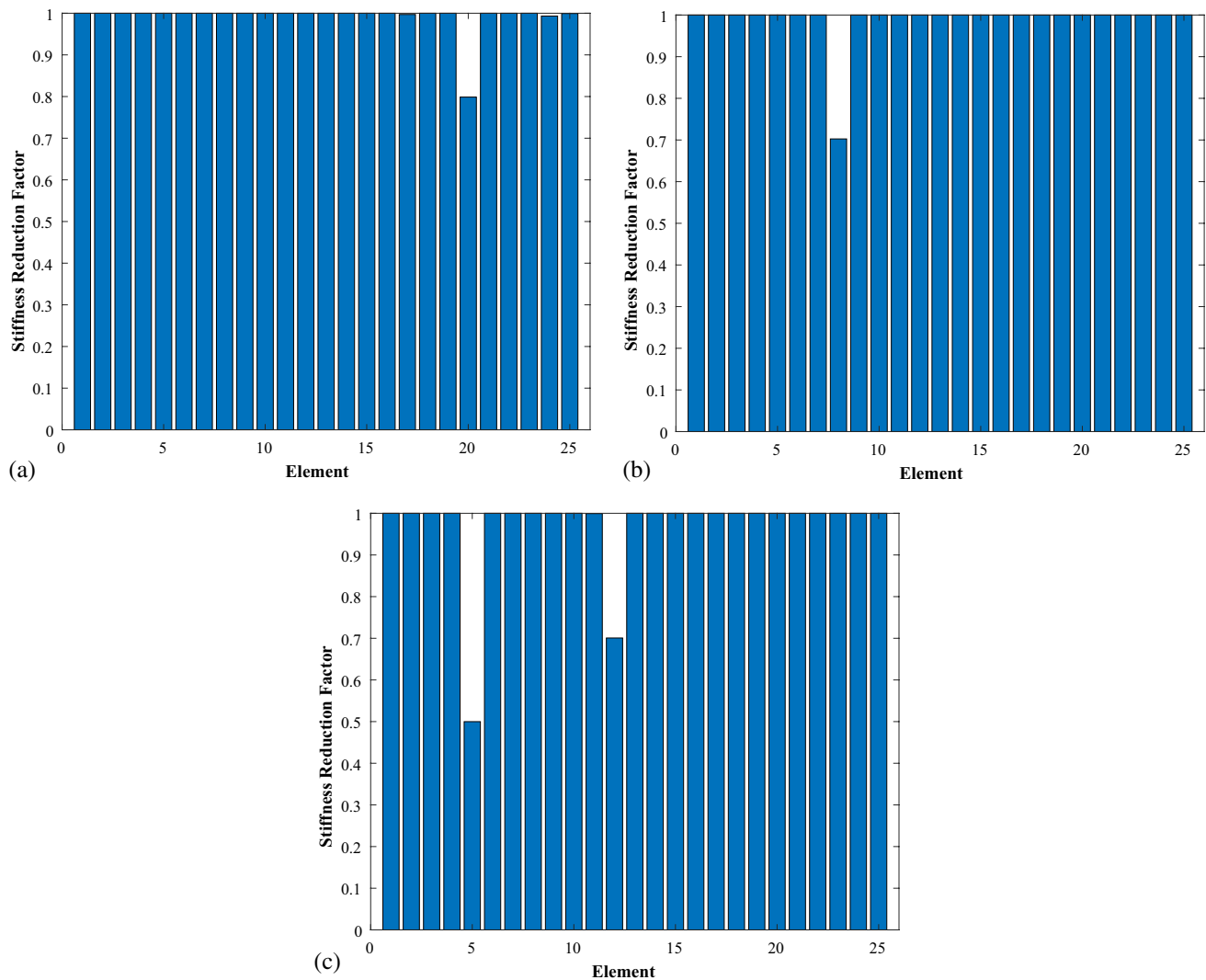


Fig. 3 Numerical beam – 3% noise: **a** damage case 1, **b** damage case 2, **c** damage case 3

The damage cases have been proposed to evaluate the influence of the position and intensity of the damage on the assertiveness of the methodology. These cases include two single damage cases and three multiple damage cases, as follows: (1) bar 7 with 20% stiffness reduction; (2) bar 54 with 20% stiffness reduction; (3) bars 26 and 27 with, respectively, 30% and 20% stiffness reduction; (4) bars 5 and 46 with, respectively, 30% and 20% stiffness reduction; (5) bars 7, 45 and 52 with, respectively, 40%, 30%, and 30% stiffness reduction.

To analyze the variation of modal parameters in the stochastic system identification and the robustness of the damage detection methodology, 3% and 5% were considered noise levels in the acceleration signals. The damage detection of the footbridge relied on data from the initial five structure modes. Table 6 shows the natural frequencies of the FE model, while Tables 7 and 8 present the frequencies generated by SSI-DATA according to the noise levels.

The damage detection method used 100 search agents in 500 iterations. Figures 7 and 8 contain the solutions of this method for the cases analyzed according to the noise levels considered. The damage was measured correctly in all cases, with disturbances being verified only in Case 5 with 5% noise. However, these irregularities identified in bars 4, 14, 40, 44, and 47 were around 1.6%, a disregarded error.

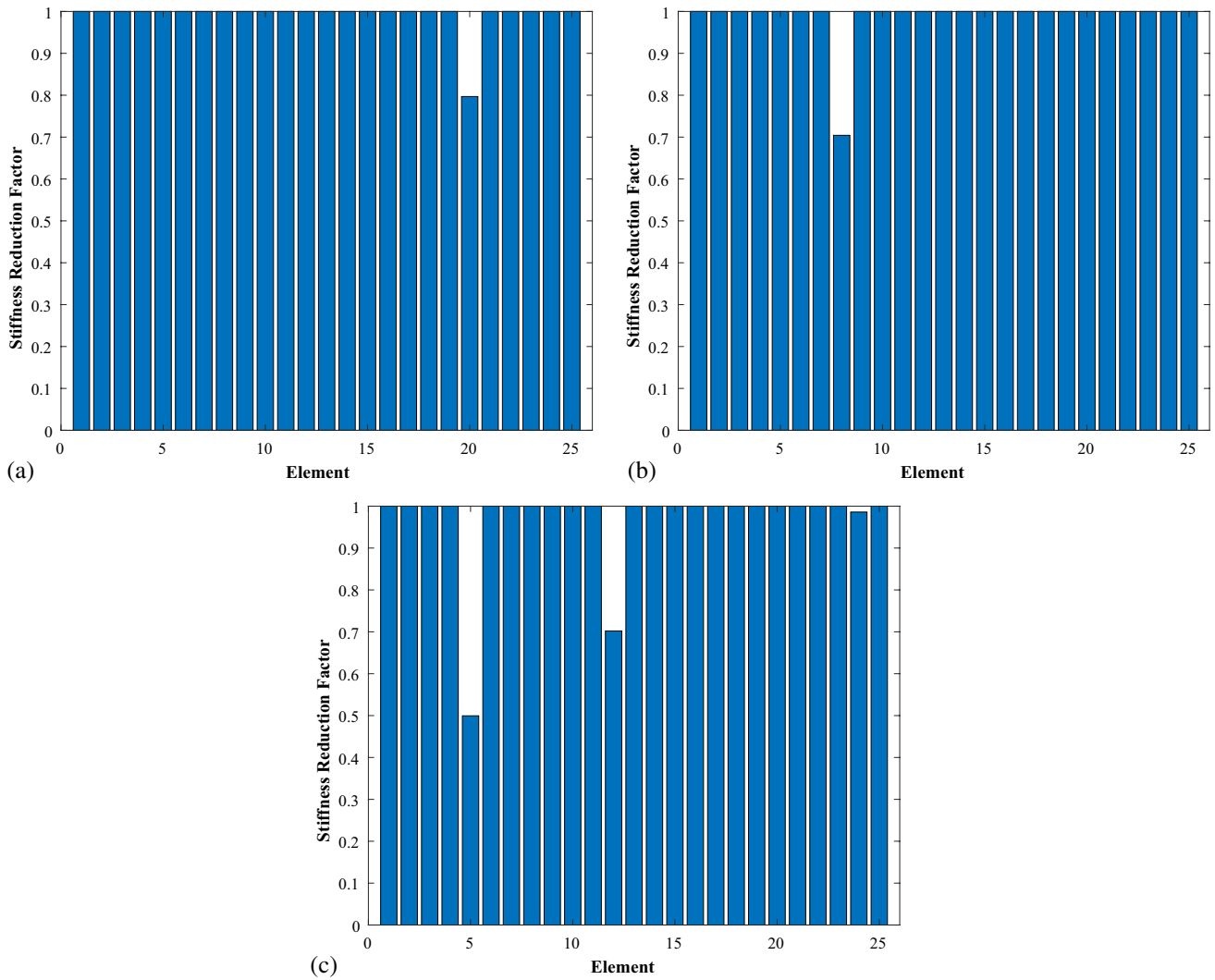
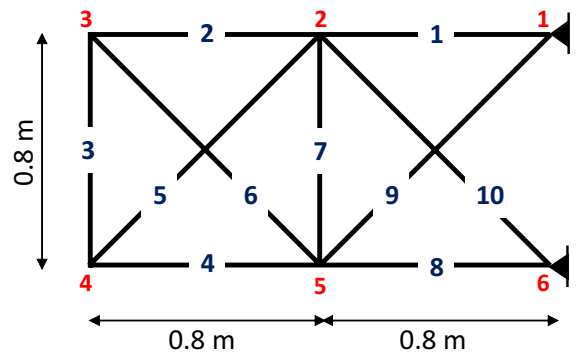


Fig. 4 Numerical beam – 5% noise: **a** damage case 1, **b** damage case 2, **c** damage case 3

Fig. 5 Numerical truss



4 Experimental structure

The damage detection methodology was further verified through experimental testing on a steel cantilever beam within the Applied Mechanics Group at the Federal University of Rio Grande do Sul. The structure, depicted in Fig. 9a, measures 39.5 mm in width, 420 mm in length, and 1.2 mm in thickness. Its material properties include a Young's

Table 3 Numerical truss structure: natural frequencies (Hz)

Mode	FE model		SSI-DATA	
	Healthy case	Damage case	Healthy case	Damage case
1	174.9996	170.5968	174.8116	170.4073
2	500.6687	484.7274	496.6709	480.9747
3	600.8525	593.0745	593.8417	586.3163

Table 4 Numerical truss structure: damage detection results

Bar	Exact damage	Predicted damage		
		Begambre and Laier [45]	Fadel Miguel et al. [16]	WOA
1	1	1	0.9995	1
2	0.85	0.8476	0.8537	0.8509
3	1	0.9987	1	1
4	1	0.9862	0.9998	1
5	1	0.9829	0.9946	1
6	1	0.9992	1	1
7	1	1	1	1
8	0.85	0.8503	0.8500	0.8508
9	1	0.9996	1	1
10	1	1	1	1

modulus of 210 GPa, a Timoshenko shear factor of 0.5, a specific mass of 8193.9 kg/m³, and a Poisson’s ratio of 0.3. The structural model utilized for this system comprised 28 Timoshenko beam elements, as illustrated in Fig. 9b.

Cuts were made in some elements in the laterals to simulate damage. The analyzed cases included: (1) reducing the width of element 13 to 33 mm; (2) reducing the width of element 13 to 18.5 mm; (3) reducing the widths of elements 8 and 13 to 17.5 mm and 18.5 mm, respectively. The experimental tests were repeated at each progressive damage step.

4.1 Vibration testing

Vibration tests were conducted under a reference condition for subsequent differentiation with damage cases using the acquisition system Pulse 12 channel Brüel & Kjær Type 3560 C. Figure 10 illustrates the experimental setup with three accelerometers whose specifications are detailed in Table 9.

To experimentally determine the modal parameters, the beam was subjected to small displacements, inducing free vibration of the system (Fig. 11). Dynamic tests were conducted at each stage, with accelerograms acquired during each repetition.

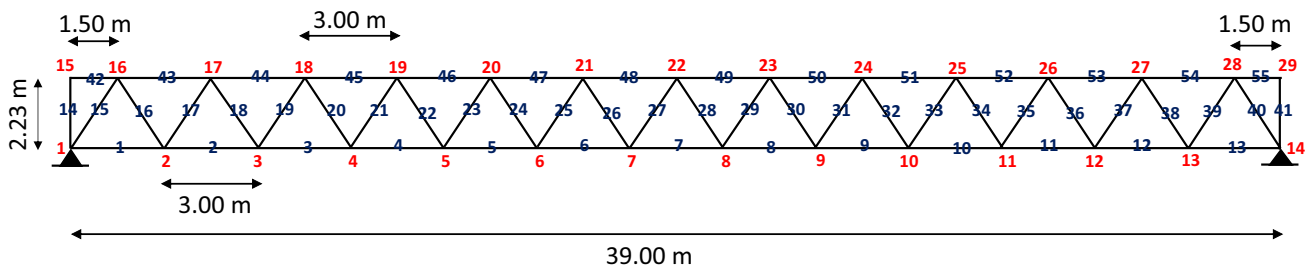


Fig. 6 Warren truss footbridge

Table 5 Numerical footbridge: bars cross-sectional area

Group	Element number	Area (m ²)
Inferior chord	1–13	0.0060
Diagonals	14–41	0.0040
Superior chord	42–55	0.0080

Table 6 Numerical footbridge: natural frequencies (Hz)

Mode	FE model					
	Healthy case	Case 1	Case 2	Case 3	Case 4	Case 5
1	5.9960	5.9820	5.9914	5.9956	5.9305	5.8432
2	16.0362	16.0362	16.0165	15.9580	15.8068	15.7378
3	33.9157	33.5875	33.8185	33.8582	33.8292	32.4809
4	41.2447	41.2447	41.2422	41.1463	41.0693	40.8871
5	55.9769	55.9769	55.7379	55.5528	55.4004	55.5217

Table 7 Numerical footbridge: identified natural frequencies with 3% noise (Hz)

Mode	SSI-DATA (3% noise)					
	Healthy case	Case 1	Case 2	Case 3	Case 4	Case 5
1	6.0096	5.9954	6.0049	6.0092	5.9414	5.8527
2	16.0398	16.0398	16.0212	15.9638	15.8050	15.7310
3	33.8875	33.5625	33.7912	33.8309	33.8013	32.4464
4	41.1606	41.1607	41.1582	41.0664	40.9921	40.8164
5	55.8083	55.8083	55.5662	55.3816	55.2281	55.3500

Table 8 Numerical footbridge: identified natural frequencies with 5% noise (Hz)

Mode	SSI-DATA (5% noise)					
	Healthy case	Case 1	Case 2	Case 3	Case 4	Case 5
1	6.0096	5.9954	6.0049	6.0092	5.9414	5.8527
2	16.0399	16.0399	16.0213	15.9640	15.8052	15.7312
3	33.8860	33.5612	33.7896	33.8294	33.7998	32.4451
4	41.1604	41.1604	41.1579	41.0662	40.9919	40.8165
5	55.8028	55.8029	55.5612	55.3772	55.2240	55.3458

4.2 Stochastic system identification

The SSI-DATA technique used each scenario's acceleration signals to calculate the first five natural frequencies precisely. Table 10 compares the numerical model frequencies and those identified from experimental data. The maximum difference observed was 2.16% at the first vibration mode.

The mode shapes identified in the healthy case are shown in Fig. 12 alongside the numerical model's mode shapes. The 4th and 5th mode shapes were not because of the limited number of three accelerometers. Nonetheless, the first three modal shapes identified exhibit a 99.99% correlation with the numerical model, as indicated by the Modal Assurance Criterion (MAC) [6] in Fig. 13. Therefore, the first five frequencies and the first three mode shapes were used for damage detection analyses.

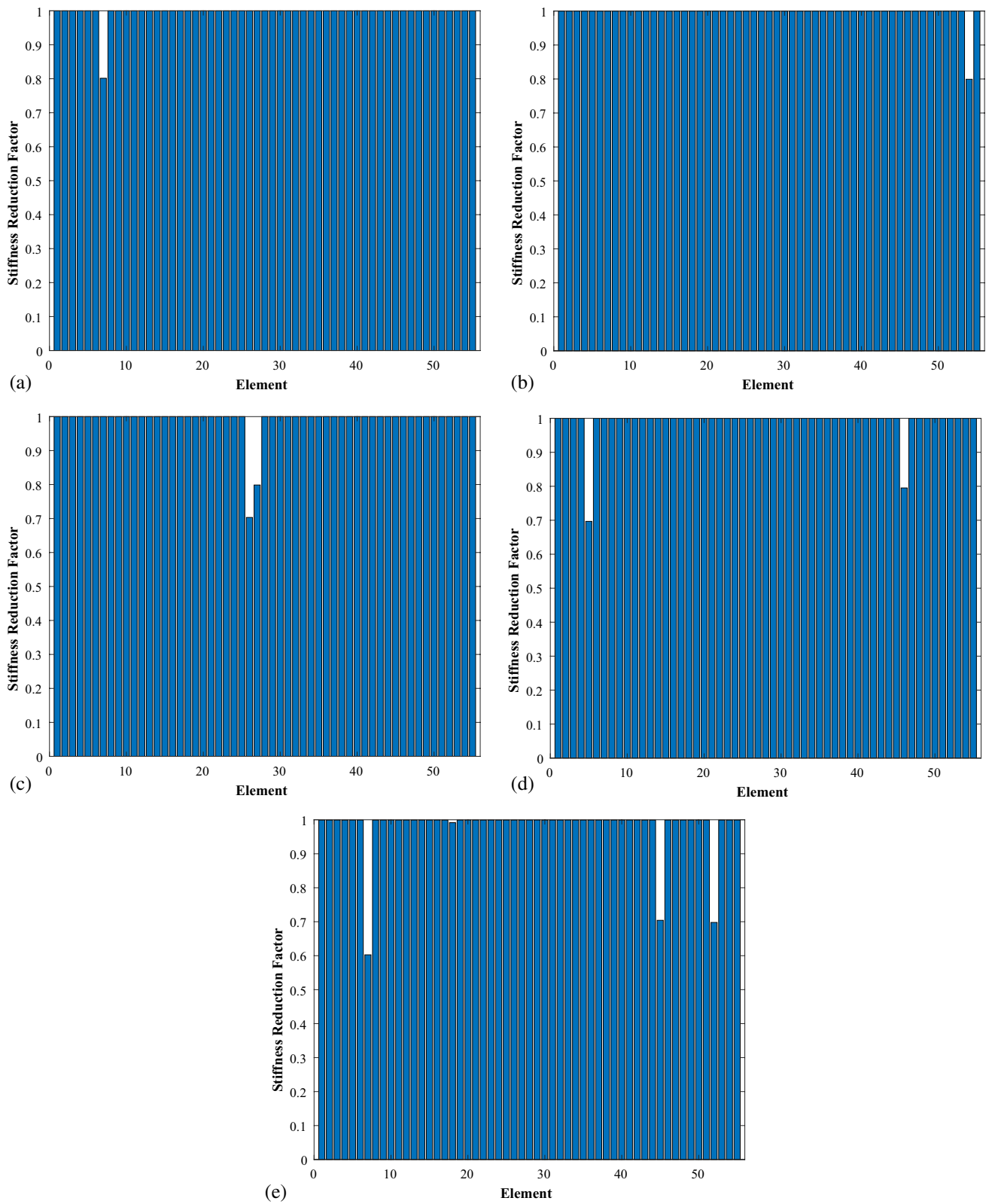


Fig. 7 Numerical footbridge – 3% noise: **a** damage case 1, **b** damage case 2, **c** damage case 3, **d** damage case 4, **e** damage case 5

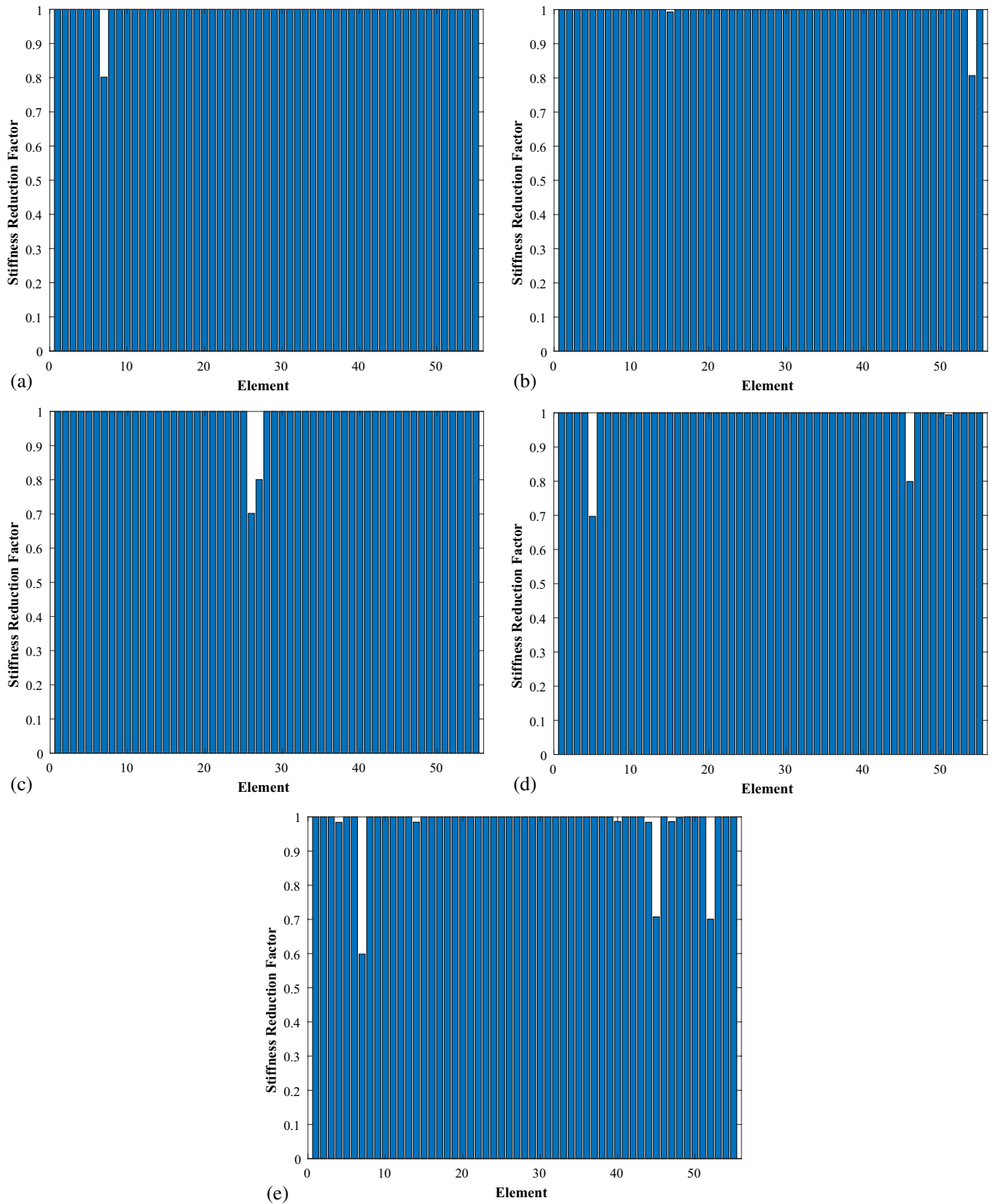


Fig. 8 Numerical footbridge – 5% noise: **a** damage case 1, **b** damage case 2, **c** damage case 3, **d** damage case 4, **e** damage case 5

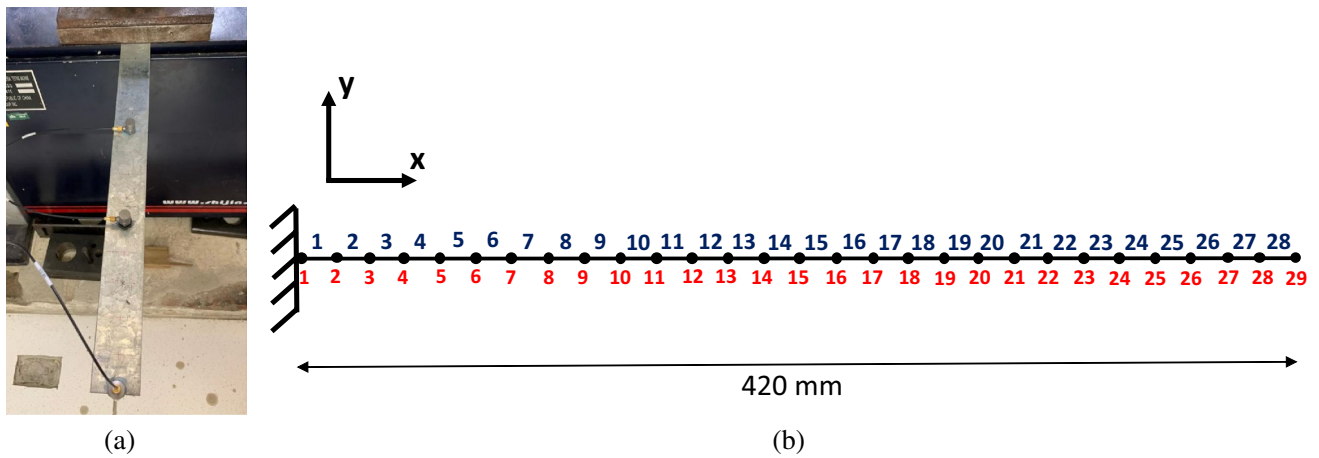


Fig. 9 Experimental structure: **a** accelerometers testing system and **b** finite elements

Fig. 10 Beam structure and experimental setup



4.3 Damage identification

Fifty search agents were used in 150 iterations to identify damage in the experimental system, yielding the results shown in Fig. 14. The methodology presented good damage localization results and a solid overall performance in quantifying damage.

5 Z24 bridge

The Z24 Bridge (Switzerland), a well-recognized realistic benchmark in the scientific community, was used as the last validation step for the presented damage detection technique. The SIMCES (System Identification to Monitor Civil Engineering Structures) chose the Z24 Bridge to develop a methodology for monitoring structural integrity. Led by the Catholic University of Leuven’s Department of Civil Engineering, Structural Mechanics Section, the structure was observed for a year, and progressive damage assessments were conducted before the bridge’s eventual demolition in 1998 [47]. This study analyzed a case involving multiple damages resulting from a pier settlement.

Table 9 Experimental setup: accelerometer data

Location	Distributor	Model	Serial number	Mass (g)
Node 11	PCB Piezotronics	352C33	86702	5.631
Node 19	PCB Piezotronics	352C33	86703	7.949
Node 29	Brüel & Kjær	4514 B 4x	51467x	8.723

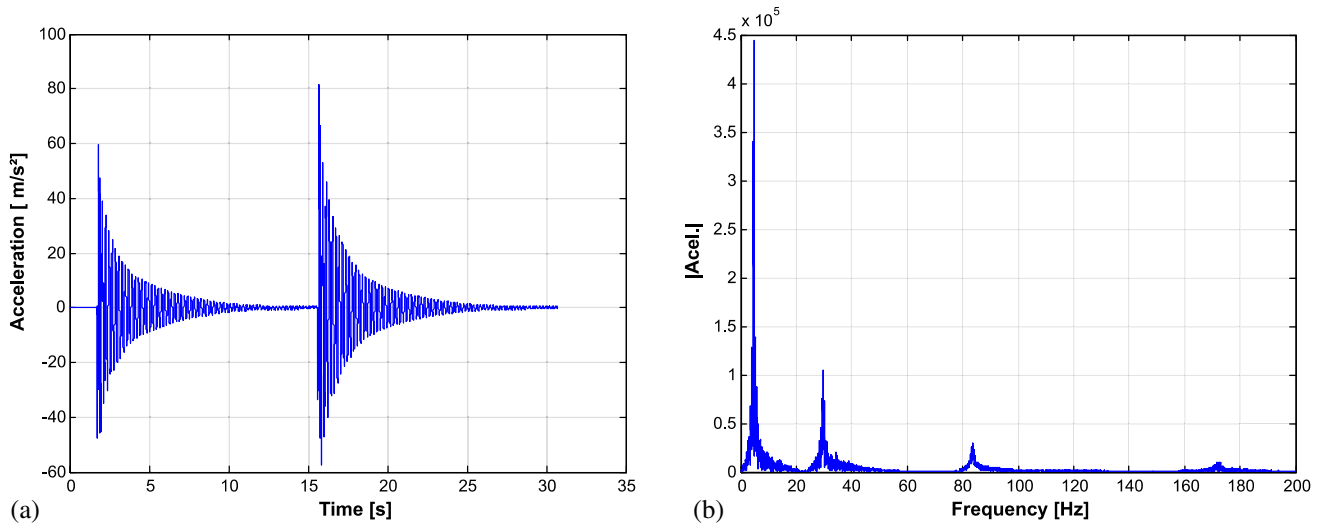


Fig. 11 Example of **a** accelerogram and **b** FFT for the experimental beam

Table 10 Experimental beam: natural frequencies (Hz)

Mode	FE model	SSI-DATA			
	Healthy case	Healthy case	Case 1	Case 2	Case 3
1	4.9341	4.8270	4.8137	4.7989	4.6853
2	30.5389	29.9510	29.9172	29.5635	29.4792
3	85.6315	85.4507	84.8619	84.7127	83.4732
4	178.8478	177.6512	176.5049	175.2284	171.8705
5	281.9240	277.3123	275.5140	275.4523	273.9630

Situated in the Canton of Bern, Switzerland, the Z24 Bridge connected Koppigen and Utzenstorf. Comprising three spans and two lanes, the bridge measured approximately 60 m in length (Fig. 15). The two central piers were firmly affixed to the girders, while pairs of columns at both ends provided support, resulting in a slightly skewed configuration [48]. The girder structure was a two-box cell constructed with post-tensioned concrete (Fig. 16).

A total of 17 progressive damage tests (PDTs) were conducted, with comprehensive descriptions provided by [49–51]. The initial set of PDTs focused on the foundation settlement of the Koppigen pier. These cases involved simulating settlement by lowering the pier ($x=44$ m), resulting in numerous girder cracks, as depicted in Fig. 17. In this study, PDT 2 was designated as the baseline healthy case, while PDT 6, representing a 95 mm settlement of the column, served as the damaged case.

5.1 Stochastic system identification

The Z24 Bridge natural frequencies were determined through the ambient vibration signals, which utilized a setup consisting of 9 configurations with two triaxial accelerometers on a pier, fifteen accelerometers on the deck (2 triaxial, three biaxial, and ten uniaxial sensors), along with three reference accelerometers (1 triaxial and two uniaxial). This setup generated a comprehensive dataset of 33 recordings at a sampling rate of 100 Hz over 655.36 s. The natural frequencies identified via the SSI-DATA technique for both healthy and damaged cases are shown in Table 11.

5.2 Finite element model updating

The FE model employed in this study was developed by [52, 53], utilizing ANSYS [54] with beam elements (with 6 degrees of freedom per node). The girder was discretized with 82 beam elements, while the piers, columns, and abutments were represented by 44 beam elements, as illustrated in Fig. 18. Additionally, mass elements were incorporated

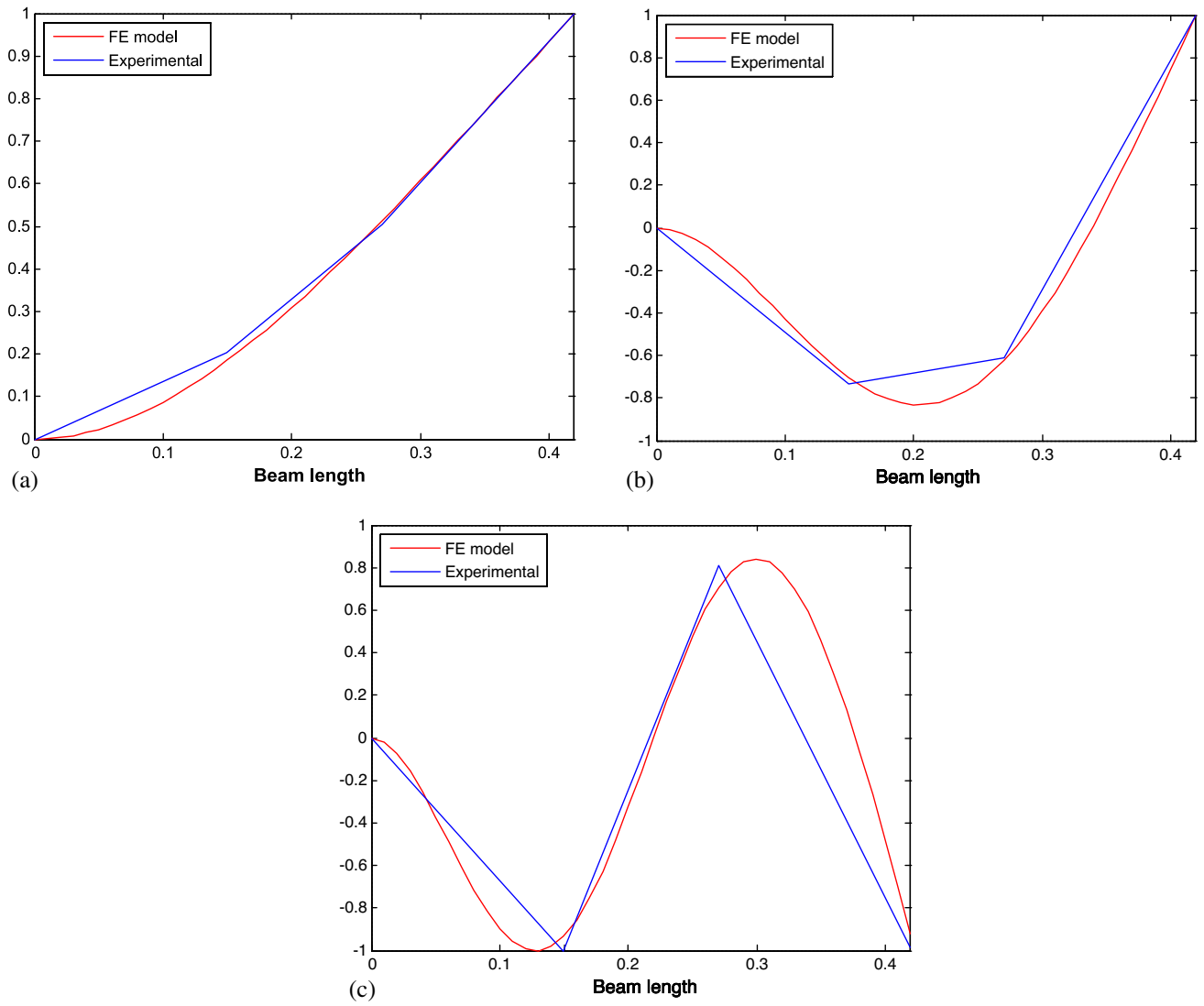
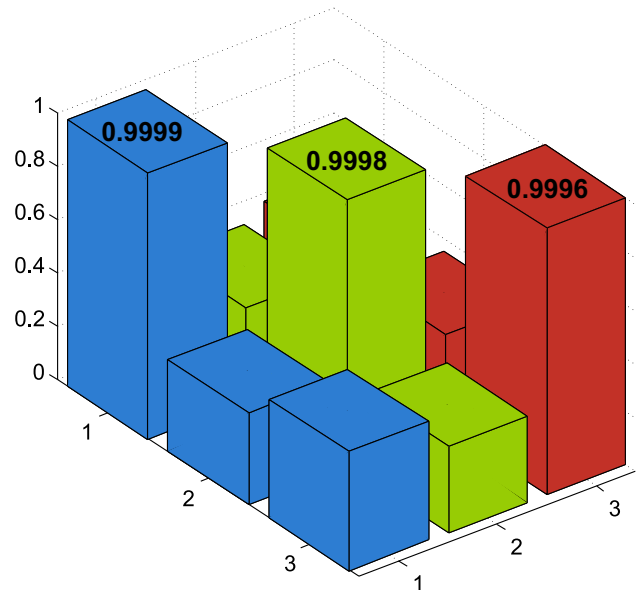


Fig. 12 Mode shapes of the system: **a** mode 1, **b** mode 2, **c** mode 3

Fig. 13 MAC for the numerical and experimental systems in the healthy case



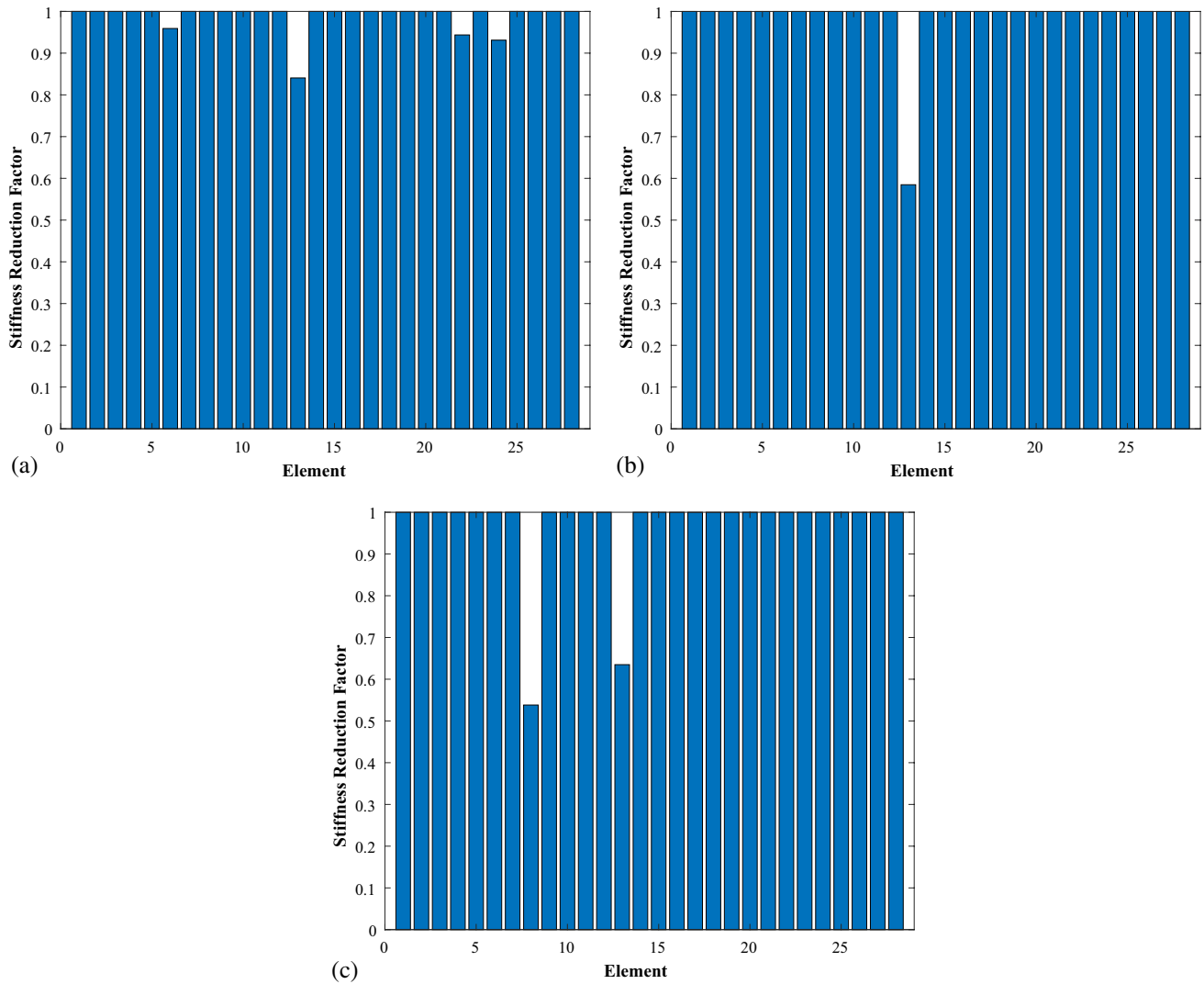
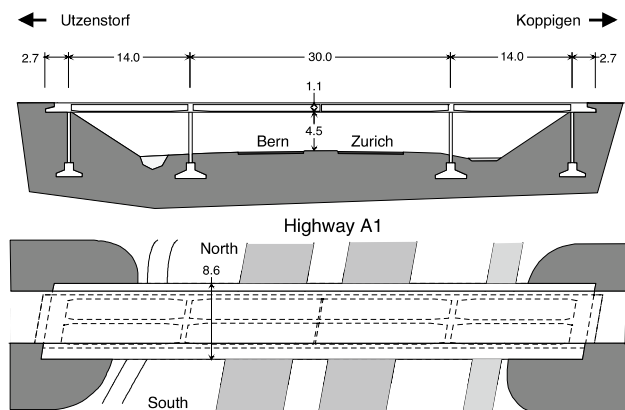


Fig. 14 Experimental beam: **a** damage case 1, **b** damage case 2, **c** damage case 3

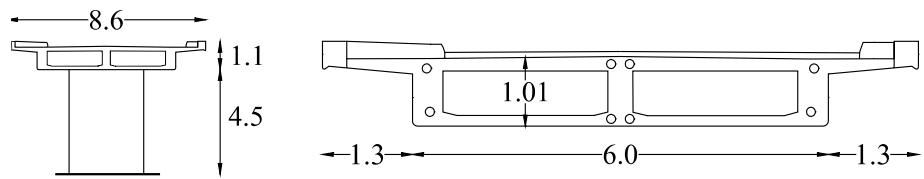
Fig. 15 Z24 Bridge: geometric information



to simulate the cross girders and foundations, accounting for concentrated translational mass and rotary inertial components.

Initially, Young's modulus $E_0 = 37.5$ GPa and shear modulus $G_0 = 20$ GPa were considered. To incorporate the soil's impact on the system, spring elements were introduced around the pillars and at the abutments' base. The soil

Fig. 16 Cross-section of the Z24 Bridge



stiffness parameters for the springs were as follows: $K_{v,p} = 180 \times 10^6 \text{ N/m}^3$ and $K_{h,p} = 210 \times 10^6 \text{ N/m}^3$ (under the piers, at $x = 14$ and 44 m); $K_{v,c} = K_{h,c} = 100 \times 10^6 \text{ N/m}^3$ (under the columns, at $x = 0$ and 58 m); $K_{v,a} = 180 \times 10^6 \text{ N/m}^3$, and $K_{h,a} = 200 \times 10^6 \text{ N/m}^3$ (at the abutments); $K_{v,ac} = K_{h,ac} = 100 \times 10^6 \text{ N/m}^3$ (around the columns).

Subsequently, the model was updated with revised values for Young’s modulus and shear modulus for the bridge girder, as well as the soil stiffness parameters, using the six natural frequencies identified in the healthy case (Table 11). This update was achieved by solving a minimization problem using the WOA and the objective function:

$$\Pi(\theta) = \sum_{j=1}^{N_m} \frac{1}{2} \left(\frac{\omega_j^2(\theta) - \tilde{\omega}_j^2}{\tilde{\omega}_j^2} \right)^2, \tag{9}$$

in which $\tilde{\omega}_j$ represents the identified natural frequency of the j th mode and ω_j denotes the natural frequency j of the numerical model as a function of the variable Φ . The parameters selected for updating during the model calibration include Young’s modulus and shear modulus for specific elements of the bridge girder, as well as key soil stiffness parameters. Out of the 82 elements comprising the bridge girder, only 17 were chosen for direct updates to their modulus values, while the modulus values for the remaining elements were interpolated based on these updated values. In total,

Fig. 17 Z24 Bridge cracks after lowering the pier

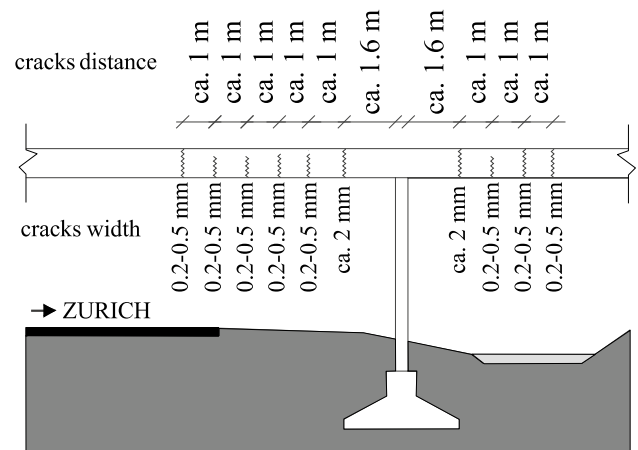
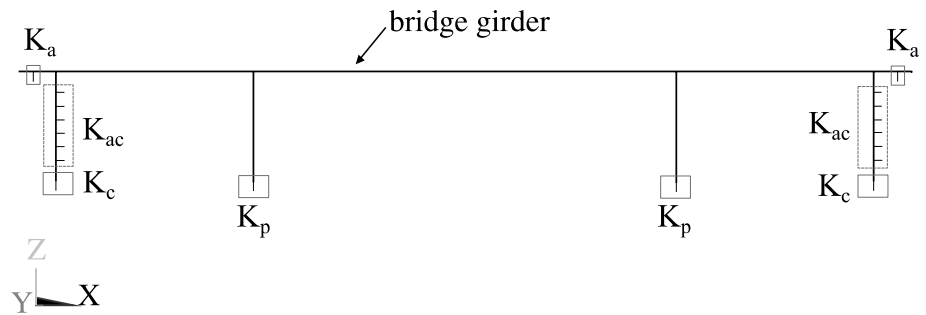


Table 11 Z24 Bridge: identified natural frequencies (Hz)

Mode	SSI-DATA		Difference (%)
	Healthy case	Damage case	
1	3.87	3.66	5.65
2	5.01	4.92	1.73
3	9.79	9.24	5.56
4	10.31	9.68	6.09
5	12.79	12.15	4.99
6	13.50	13.44	0.44

Fig. 18 Z24 Bridge: FE model



36 variables were updated: 17 shear moduli and 17 Young’s moduli for the bridge girder, along with the horizontal stiffness under the abutments ($K_{h,a}$) and the vertical soil stiffness under the piers ($K_{v,p}$).

As indicated in Table 12, the discrepancy between the first six experimental frequencies and the revised numerical frequencies was under 1%. The updated soil stiffness parameters were $K_{v,p} = 147.5 \times 10^6 \text{ N/m}^3$, and $K_{h,a} = 146.4 \times 10^6 \text{ N/m}^3$. Figure 19 compares the initial model values and the updated bending stiffness (EI_y) and torsional stiffness (GI_x) parameters.

5.3 Damage identification

In the updated finite element model, nine regions of the girder were defined (as illustrated in Fig. 20) to decrease the amount of stiffness reduction factors and computational time to assess the bridge. These regions characterize the influence zones of the piers, abutments, and girder partitions.

For the Z24 Bridge, the damage detection methodology solely employed the initial part of Eq. (3). Therefore, the objective function of this approach focused exclusively on minimizing the disparity between healthy and damaged natural frequencies without considering the mode shapes. The WOA used 30 search agents in 60 iterations, and the solution of the method is shown in Fig. 21.

Regarding the Z24 Bridge, the presented approach successfully located the primary damaged zone (region 7), coinciding with the pier settlement and cracks in the neighboring areas. Additionally, it identified secondary damage zones resulting from cracking alongside the pier (regions 6 and 8). The identified damage levels could not be verified due to the absence of accurate quantitative response data.

The results in Fig. 21 exhibit better overall performance compared to previous works. For example, in Sony et al. [55], the lack of quantitative data regarding physical parameters within the damage index impeded the inference of damage without comprehensively assessing each structural element across the damage cases. Moreover, Masciotta et al. [56] achieved fair outcomes using five points within the spectral damage localization index. These indexes corresponded to the bridge’s zones, approximately half the number used in this paper. In the work of Monteiro et al. [21], the output factor (damage index) can be interpreted as analogous to this work’s stiffness reduction factor. However, the damage detection method via Artificial Neural Networks used by [21] could not identify damage in region 8. Finally, in model-based approaches such as those by Teughels and De Roeck [52] and Reynders et al. [53], the bridge girder was divided into eight elements for damage assessment. While these studies calculated correction factors (damage index) for the Young’s and shear modulus, the results for damage localization and quantification were presented in a format that made direct comparison challenging, as both types of correction factors were not

Table 12 Z24 Bridge: updated numerical frequencies

Vibration mode	Finite element model		SSI-DATA	Difference (%)
	Initial	Updated		
1	3.73	3.86	3.87	- 0.26
2	5.14	5.04	5.01	0.70
3	9.64	9.75	9.79	- 0.33
4	10.25	10.37	10.31	0.52
5	12.52	12.81	12.79	0.14
6	13.35	13.39	13.50	- 0.85

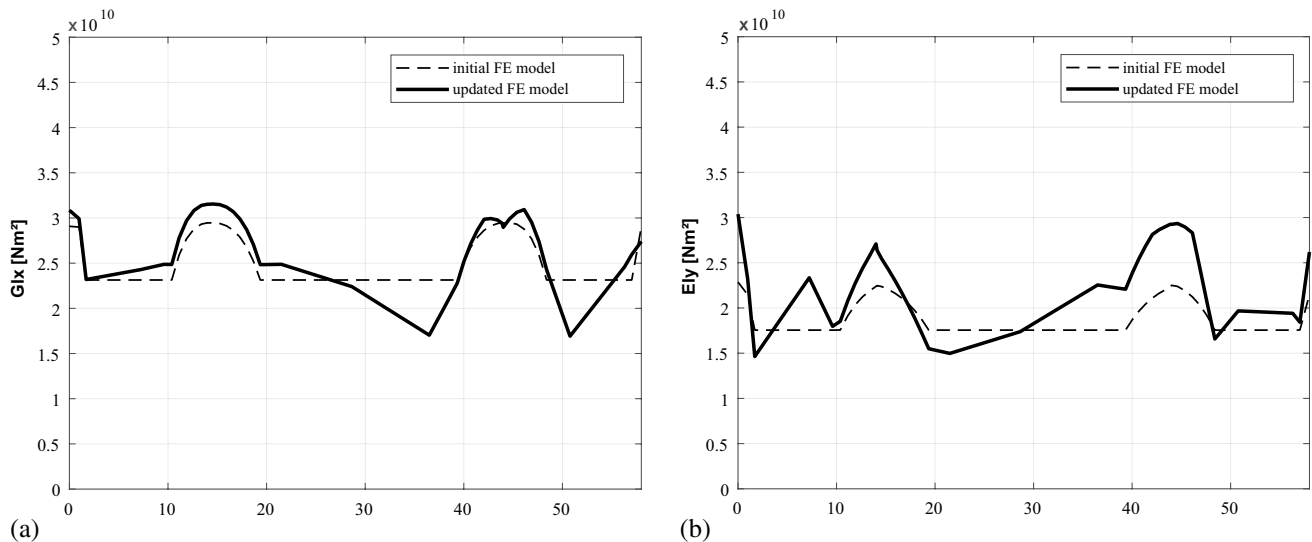


Fig. 19 Updating values: **a** torsional stiffness distribution, **b** bending stiffness distribution

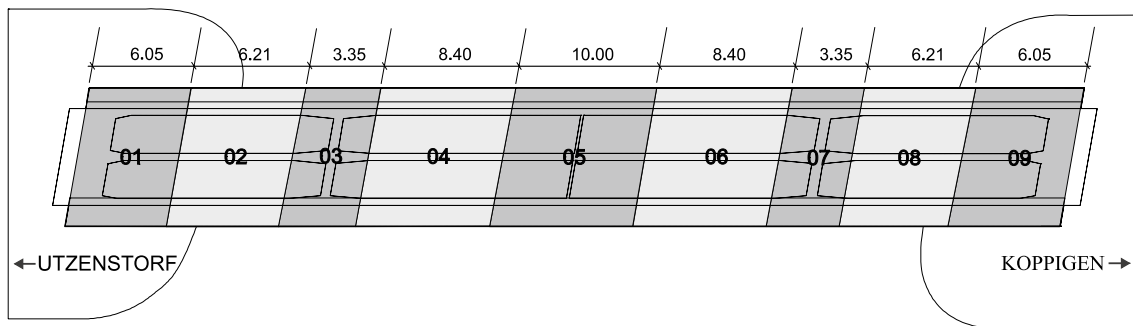


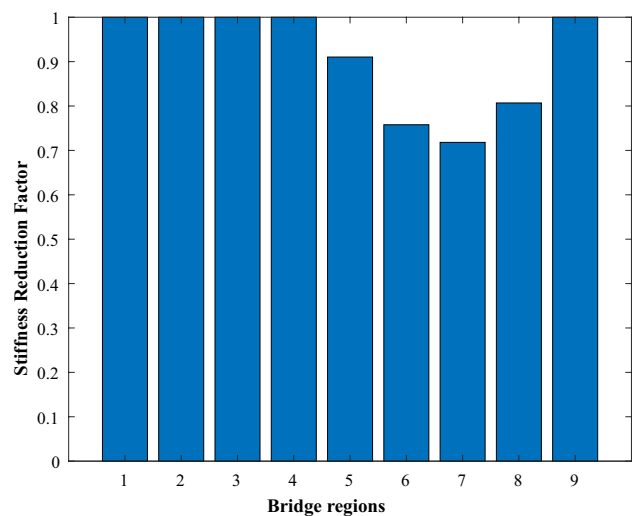
Fig. 20 Z24 Bridge regions

completely aligned with each other. In other words, Teughels and De Roeck [52] and Reynders et al. [53] did not provide a unified damage index to localize and quantify damage.

6 Final remarks

This paper presented an approach for damage detection based on matrix updating through the Whale Optimization Algorithm. The methodology was assessed through both numerical simulations and experimental tests. Three numerical examples (cantilever beam, truss, and footbridge) and two experimental structures (cantilever beam and Z24 Bridge) were analyzed using the proposed methodology. This comprehensive analysis facilitated the evaluation of the performance of the proposed method in identifying, locating, and quantifying single and multiple damage cases. The results yielded the following conclusions:

Fig. 21 Z24 Bridge damage detection



- The WOA proved to be a useful tool not only for detecting damage but also for locating and quantifying damage in structures through the method based on matrix updating while considering the presence of noise in the signals. In addition, it found better results than those found by other authors in the literature who also studied the same numerical examples.
- The proposed approach effectively identified, located, and quantified single and multiple damages in the experimental tests conducted on the steel beam.
- The study on the Z24 Bridge demonstrated the method's efficacy in locating damage, validating its applicability to real civil structures. Moreover, even when relying solely on natural frequencies for evaluation, the method successfully estimated the damage resulting from pier settlement.
- The presented framework used simplified calibrated finite element models, such as bar or beam elements, making this approach accessible for practical engineering applications where computational resources may be limited. This advantage is particularly relevant for large-scale structures, where more complex models could be computationally prohibitive.

Acknowledgements The authors acknowledge the KU Leuven Structural Mechanics Section as the source of the Z24 Bridge data.

Author contributions All authors contributed to the present study. Material preparation, data collection, and analysis were performed by DKM, LFFM, GZ, TB, GSA, and RRB. The first draft of the manuscript was written by DKM and LFFM, and all authors commented on previous versions of the manuscript. All authors read and approved the final manuscript.

Funding This research was supported by *Conselho Nacional de Desenvolvimento Científico e Tecnológico* (CNPq) and *Coordenação de Aperfeiçoamento de Pessoal de Nível Superior* (CAPES), Brazil.

Data availability The data supporting this research are available upon request.

Code availability The codes developed in this research are available upon reasonable request to the corresponding author.

Declarations

Competing interests The authors declare no competing interests.

Open Access This article is licensed under a Creative Commons Attribution-NonCommercial-NoDerivatives 4.0 International License, which permits any non-commercial use, sharing, distribution and reproduction in any medium or format, as long as you give appropriate credit to the original author(s) and the source, provide a link to the Creative Commons licence, and indicate if you modified the licensed material. You do not have permission under this licence to share adapted material derived from this article or parts of it. The images or other third party material in this article are included in the article's Creative Commons licence, unless indicated otherwise in a credit line to the material. If material is not included in the article's Creative Commons licence and your intended use is not permitted by statutory regulation or exceeds the permitted use, you will need to obtain permission directly from the copyright holder. To view a copy of this licence, visit <http://creativecommons.org/licenses/by-nc-nd/4.0/>.

References

1. Juang JN, Pappa RS. An eigensystem realization algorithm for modal parameter identification and model reduction. *J Guid Control Dyn.* 1985;8(5):620–7. <https://doi.org/10.2514/3.20031>.
2. Van Overschee P, De Moor B. Subspace identification for linear systems: theory-implementation-applications. Leuven: Kluwer Academic Publishers; 1996.
3. Peeters B, Van Der Auweraer H. PolyMAX: a revolution in operational modal analysis. Proceedings of the International Operational Modal Analysis Conference, IOMAC; 2005.
4. Salawu OS. Detection of structural damage through changes in frequency a review. *Eng Struct.* 1997. [https://doi.org/10.1016/S0141-0296\(96\)00149-6](https://doi.org/10.1016/S0141-0296(96)00149-6).
5. Allemang RJ and Brown DL. A correlation coefficient for modal vector analysis. Proceedings of the 1st International Modal Analysis Conference, IMAC 1982.
6. Curadelli RO, Riera JD, Ambrosini D, Amani MG. Damage detection by means of structural damping identification. *Eng Struct.* 2008. <https://doi.org/10.1016/j.engstruct.2008.05.024>.
7. Bakhshizadeh A, Sadeghi K, Ahmadi S, Royaei J. Damage identification in long-span cable-stayed bridges under multiple support excitations. *Int J Civil Engin.* 2023. <https://doi.org/10.1007/s40999-023-00823-7>.
8. Abdel Wahab MM, De Roeck G. Damage detection in bridges using modal curvatures: application to a real damage scenario. *J Sound Vib.* 1999. <https://doi.org/10.1006/jsvi.1999.2295>.
9. Baneen U, Kausar Z. A baseline-free modal strain energy method for damage localisation. *Int J Civil Engin.* 2018. <https://doi.org/10.1007/s40999-017-0149-z>.
10. He WU, Ren WX, Cao L, Wang Q. FEM free damage detection of beam structures using the deflections estimated by modal flexibility matrix. *Int J Struct Stab Dyn.* 2021. <https://doi.org/10.1142/S0219455421501285>.
11. Fadel Miguel LF, Miguel LFF, Riera JD, Ramos de Menezes RC. Damage detection in truss structures using a flexibility based approach with noise influence consideration. *Struct Engin Mech.* 2007. <https://doi.org/10.12989/sem.2007.27.5.625>.
12. Prudencio EE, Bauman PT, Faghihi D, Ravi-Chandar K, Oden JT. A computational framework for dynamic data-driven material damage control, based on Bayesian inference and model selection. *Int J Numer Meth Eng.* 2014. <https://doi.org/10.1002/nme.4669>.
13. Zheng W, Shen J, Wang J. Improved computational framework for efficient bayesian probabilistic inference of damage in truss structures based on vibration measurements. *Transp Res Rec.* 2014. <https://doi.org/10.3141/2460-13>.
14. Zhu B, Leung AYT, Wong CK, Lu WH. On-line health monitoring and damage detection of structures based on the wavelet transform. *Int J Struct Stab Dyn.* 2008. <https://doi.org/10.1142/S0219455408002703>.
15. Altammar H, Dhingra A, Kaul S. Use of wavelets for mixed-mode damage diagnostics in warren truss structures. Proceedings of the ASME 2014 international design engineering technical conferences & computers and information in engineering conference, IDETC/CIE. 2014.
16. Fadel Miguel LF, Lopez RH, Miguel LFF. A hybrid approach for damage detection of structures under operational condition. *J Sound Vib.* 2013. <https://doi.org/10.1016/j.jsv.2013.03.017>.
17. Fadel Miguel LF, Miguel LFF, Kaminski J Jr, Riera JD. Damage detection under ambient vibration by harmony search algorithm. *Expert Syst Appl.* 2012. <https://doi.org/10.1016/j.eswa.2012.02.147>.
18. Fadel Miguel LF, Miguel LFF, Kaminski J Jr. Stochastic system identification and damage detection using firefly algorithm. *Int J Lifecycle Perform Engin.* 2014. <https://doi.org/10.1504/IJLCP.2014.064104>.
19. Jiang S, Chen W, Sun L, Du C. Flaw classification and detection in thin-plate structures based on scaled boundary finite element method and deep learning. *Int J Numer Meth Eng.* 2022. <https://doi.org/10.1002/nme.7051>.
20. Mehrjoo M, Khaji N, Moharrami H, Bahreininejad A. Bahreininejad, damage detection of truss bridge joints using artificial neural networks. *Expert Syst Appl.* 2008. <https://doi.org/10.1016/j.eswa.2007.08.008>.
21. Monteiro DK, Miguel LFF, Zeni G, Becker T, de Andrade GS, de Barros RR. Detection, localization, and quantification of damage in structures via artificial neural networks. *Shock Vib.* 2023. <https://doi.org/10.1155/2023/8829298>.
22. Ghannadi P, Kourehli SS. An effective method for damage assessment based on limited measured locations in skeletal structures. *Adv Struct Eng.* 2021. <https://doi.org/10.1177/1369433220947193>.
23. Kourehli SS. Structural damage diagnosis using incomplete static responses and LS-SVM. *Inverse Probl Sci Engin.* 2017. <https://doi.org/10.1080/17415977.2016.1169277>.
24. Doebling SW, Farrar CR, Prime ME, Shevitz DW. Damage identification and health monitoring of structural and mechanical systems from changes in their vibration characteristics: a literature review. Los Alamos: Los Alamos National Lab(LANL); 1996.
25. Fan W, Qiao P. Vibration-based damage identification methods: a review and comparative study. *Struct Health Monit.* 2011. <https://doi.org/10.1177/1475921710365419>.
26. An Y, Chatzi E, Sim S-H, Laflamme S, Blachowski B, Ou J. Recent progress and future trends on damage identification methods for bridge structures. *Struct Control Health Monit.* 2019. <https://doi.org/10.1002/stc.2416>.
27. Rytter A. Vibrational based inspection of civil engineering structures. Ph.D. dissertation—department of building technology and structural engineering. Aalborg: Aalborg University; 1993.
28. Ghannadi P, Kourehli SS. Data-driven method of damage detection using sparse sensors installation by SEREPa. *J Civ Struct Heal Monit.* 2019. <https://doi.org/10.1007/s13349-019-00345-8>.
29. Ghannadi P, Kourehli SS, Noori M, Altabay WA. Efficiency of grey wolf optimization algorithm for damage detection of skeletal structures via expanded mode shapes. *Adv Struct Eng.* 2020. <https://doi.org/10.1177/1369433220921000>.
30. Sang-To T, Le-Minh H, Mirjalili S, Wahab MA. A new movement strategy of grey wolf optimizer for optimization problems and structural damage identification. *Adv Eng Softw.* 2022. <https://doi.org/10.1016/j.advengsoft.2022.103276>.
31. Frans R, Arfiadi Y. Damage detection in space truss structures using a third-level approach. *Dis Civil Engin.* 2024. <https://doi.org/10.1007/s44290-024-00013-x>.

32. Ghannadi P, Kourehli SS, Mirjalili S. The application of PSO in structural damage detection: an analysis of the previously released publications (2005–2020). *Frattura Ed Integrità Strutturale*. 2022. <https://doi.org/10.3221/IGF-ESIS.62.32>.
33. Ghannadi P, Kourehli SS. Multiverse optimizer for structural damage detection: numerical study and experimental validation. *Struct Design Tall Spec Build*. 2020. <https://doi.org/10.1002/tal.1777>.
34. Zeni G. Detecção de dano em estruturas utilizando identificação modal estocástica e um algoritmo de otimização. Master dissertation—programa de pós-graduação em engenharia mecânica. Porto Alegre: Universidade Federal do Rio Grande do Sul, PROMEC/UFRGS; 2018.
35. Miguel LFF, dos Santos GP. Optimization of multiple tuned mass dampers for road bridges taking into account bridge-vehicle interaction, random pavement roughness, and uncertainties. *Shock Vib*. 2021. <https://doi.org/10.1155/2021/6620427>.
36. Brito JWS, Miguel LFF. Optimization of a reinforced concrete structure subjected to dynamic wind action. *Frattura Ed Integrità Strutturale*. 2021. <https://doi.org/10.3221/IGF-ESIS.59.22>.
37. Brandão FS, Almeida AK, Miguel LFF. Optimum design of single and multiple tuned mass dampers for vibration control in buildings under seismic excitation. *Int J Struct Stab Dyn*. 2022. <https://doi.org/10.1142/S021945542250078X>.
38. Ontiveros-Pérez SP, Miguel LFF. Reliability-based optimum design of multiple tuned mass dampers for minimization of the probability of failure of buildings under earthquakes. *Structures*. 2022. <https://doi.org/10.1016/j.istruc.2022.06.015>.
39. de Souza OAP, Miguel LFF. CIOA: circle-inspired optimization algorithm, an algorithm for engineering optimization. *SoftwareX*. 2022. <https://doi.org/10.1016/j.softx.2022.101192>.
40. Mirjalili S, Lewis A. The parameters selected for updating during the model. *Adv Eng Softw*. 2016. <https://doi.org/10.1016/j.advengsoft.2016.01.008>.
41. MATLAB®. version 8.0.0.783 (r2012b), The MathWorks Inc.: Natick, Massachusetts. 2012.
42. Newmark NM. A Method for Computation of Structural Dynamics. *J Eng Mech Div*. 1959. <https://doi.org/10.1061/JMCEA3.0000098>.
43. Peeters B. System identification and damage detection in civil engineering. Ph.D. dissertation—departement burgerlijke bouwkunde. Leuven: Katholieke Universiteit Leuven; 2000.
44. Kaminski Jr J, Riera JD. Structural damage detection by means vibration test. *Proceedings of the 14th international conference on structural mechanics in reactor technology, SMIRT 14*. 1997.
45. Begambre O, Laier JE. A hybrid Particle Swarm Optimization—Simplex algorithm (PSOS) for structural damage identification. *Adv Eng Softw*. 2009. <https://doi.org/10.1016/j.advengsoft.2009.01.004>.
46. Miguel LFF, Fadel Miguel LF, Lopez RH. A firefly algorithm for the design of force and placement of friction dampers for control of man-induced vibrations in footbridges. *Optim Eng*. 2014. <https://doi.org/10.1007/s11081-014-9269-3>.
47. De Roeck G. The state-of-the-art of damage detection by vibration monitoring: the SIMCES experience. *J Struct Control*. 2003. <https://doi.org/10.1002/stc.20>.
48. Peeters B, De Roeck G. One-year monitoring of the Z24-Bridge: environmental effects versus damage events. *Earthquake Eng Struct Dynam*. 2001. [https://doi.org/10.1002/1096-9845\(200102\)30:2%3C149::AID-EQE1%3E3.0.CO;2-Z](https://doi.org/10.1002/1096-9845(200102)30:2%3C149::AID-EQE1%3E3.0.CO;2-Z).
49. Krämer C. Brite-Euram project SIMCES, Task A1 and A2: long term monitoring and bridge tests. Technical report 168'349/20e, EMPA: Dübendorf. 1999.
50. Maeck J, De Roeck G. Description of Z24 benchmark. *Mech Syst Sign Process*. 2003. <https://doi.org/10.1006/mssp.2002.1548>.
51. Reynders E, De Roeck G. Continuous vibration monitoring and progressive damage testing on the Z24 bridge. *Encyclopedia of structural health monitoring*. John Wiley & Sons: Hoboken; 2009.
52. Teughels A, De Roeck G. Structural damage identification of the highway bridge Z24 by FE model updating. *J Sound Vib*. 2004. <https://doi.org/10.1016/j.jsv.2003.10.041>.
53. Reynders E, Teughels A, De Roeck G. Finite element model updating and structural damage identification using OMAX data. *Mech Syst Signal Process*. 2010. <https://doi.org/10.1016/j.ymsp.2010.03.014>.
54. Ansys®. Academic research mechanical, Release 22.2, ANSYS, Inc. 2022.
55. Sony S, Gamage S, Sadhu A, Samarabandu J. Vibration-based multiclass damage detection and localization using long short-term memory networks. *Structures*. 2022. <https://doi.org/10.1016/j.istruc.2021.10.088>.
56. Masciotta MG, Ramos LF, Lourenço PB, Vasta M, De Roeck G. A spectrum-driven damage identification technique: application and validation through the numerical simulation of the Z24 Bridge. *Mech Syst Signal Process*. 2016. <https://doi.org/10.1016/j.ymsp.2015.08.027>.

Publisher's Note Springer Nature remains neutral with regard to jurisdictional claims in published maps and institutional affiliations.